Sub-pixel land cover classification for improved urban area estimates using Landsat

Andrew MacLachlan [1],*, Gareth Roberts [2], Eloise Biggs [3] and Bryan Boruff [4]

1 *Geography and Environment, The University of Southampton, University Road, Southampton, SO17 1BJ, UK; A.C.MacLachlan@soton.ac.uk*

2 *Geography and Environment, The University of Southampton, University Road, Southampton, SO17 1BJ, UK;G.J.Roberts@soton.ac.uk*

3 *UWA School of Agriculture and Environment, The University of Western Australia, Crawley, WA, 6009, Australia; eloise.biggs@uwa.edu.au*

4 *UWA School of Agriculture and Environment, The University of Western Australia, Crawley, WA, 6009, Australia; bryan.boruff@uwa.edu.au*

* Correspondence: A.C.MacLachlan@soton.ac.uk, +44-(0)23-8059-9586

All authors assisted in conceiving and designing the experiments lead by Andrew MacLachlan; Andrew MacLachlan performed the experiments and analysed the data; Gareth Roberts, Eloise Biggs and Bryan Boruff contributed reagents/materials/analysis tools; Andrew MacLachlan wrote the paper with input and revisions from Gareth Roberts, Eloise Biggs and Bryan Boruff.

Sub-pixel land cover classification for improved urban area estimates using Landsat

Urban areas are Earth's fastest growing land use that impact hydrological and ecological systems and the surface energy balance. The identification and extraction of accurate spatial information relating to urban areas is essential for future sustainable city planning owing to its importance within global environmental change and human-environment interactions. However, monitoring urban expansion using medium resolution (30-250m) imagery remains challenging due to the variety of surface materials that contribute to measured reflectance resulting in spectrally mixed pixels. This research integrates high spatial resolution orthophotos and Landsat imagery to identify differences across a range of diverse urban subsets within the rapidly expanding Perth Metropolitan Region, Western Australia. Results indicate that calibrating Landsat derived sub-pixel land cover estimates with correction values (calculated from spatially explicit comparisons of sub-pixel Landsat values to classified high resolution data which accounts for over (under) estimations of Landsat) reduces moderate resolution urban area over (under) estimates by on average 55.08% for the Perth Metropolitan Region. This approach can be applied to other urban areas globally through use of frequently available and/or low cost high spatial resolution imagery (e.g. using Google Earth). This will improve urban growth estimations to help monitor and measure change whilst providing metrics to facilitate sustainable urban development targets within cities around the world.

Keywords: Urban expansion, multispatial comparison, Landsat, High spatial resolution, policy

1. Introduction

Urban areas are estimated to cover only 0.5% of Earth's surface yet are one of the fastest growing land use per area basis (Schneider, Friedl, and Potere 2010; Bettencourt and West 2010; Schneider, Friedl, and Potere 2009). Population growth has resulted in increased urbanisation with 54% of the planet's seven billion people in 2014 residing in urban areas with an additional 2.5 billion urban dwellers projected by 2050, whilst

concurrently increasing the proportion of world's urban population to 66% (Sexton et al. 2013; Powell and Roberts 2010; Sharifi and Lehmann 2014; United Nations, Department of Economic and Social Affairs 2014; Powell et al. 2007; Song et al. 2016). Alteration of natural land cover to anthropogenic impervious surfaces has been identified as the most extreme cumulative effect of land cover change, generating numerous socio-economic consequences including: amenity provision efficiency, ecological degradation and the Urban Heat Island (UHI) effect (Cai et al. 2016; Howard 1988; L. Hu and Brunsell 2015; Xie and Zhou 2015). Accurate information on urban Land Cover and Land Use (LULC) is therefore imperative for monitoring expansion and planning policy targeting for future sustainable development of our cities (Bettencourt and West 2010; Wu and Murray 2003). Earth Observation (EO) enables consistent, detailed characterisation of the actual urban footprint of a city having been mapped and monitored using remotely sensed data at a range of spatial and temporal scales for associated implications (Schneider, Friedl, and Potere 2010; Imhoff et al. 1997; Sexton et al. 2013; Akbari, Rose, and Taha 2003; Friedl et al. 2002). However, accurate and consistent monitoring of urban land cover is frequently precluded by coarse spatial (e.g. 1 km^2 Moderate Resolution Imaging Spectroradiometer (MODIS) land cover product) and temporal (e.g. 2000 and 2010 GlobeLand30 product) resolution of such datasets (Song et al. 2016; Lu et al. 2014).

Urban mapping remains challenging due to the heterogeneity of surface materials and surface structure which contributes to pixel surface reflectance that are often difficult to disentangle (Herold et al. 2002; Lu, Moran, and Hetrick 2011; Varshney and Rajesh 2014; Schneider 2012). When delineating urban land cover from remotely sensed data, spatial resolution is considered the most important factor which provides increased visibility of discrete surface features (e.g. buildings) and greater

pixel homogeneity over medium to coarse spatial resolution satellite imagery (e.g. Landsat and MODIS) (Myint et al. 2011). Nevertheless, high spatial resolution data often lack temporal acquisition consistency (e.g. airborne orthophotos) or are expensive to purchase (e.g. commercial satellite imagery). Consequently, in order to best monitor urban LULC change, datasets must have an adequate spatial and temporal resolution to discern change. In this regard, data from the Landsat series of satellites provides the longest time-series of consistent, medium spatial resolution imagery that has been extensively applied to urban area mapping (Powell et al. 2007; Schneider and Mertes 2014; Sundarakumar et al. 2012; Wilson et al. 2003; Yuan et al. 2005; Song et al. 2016).

Accurate quantification of anthropogenic landscape modification is of critical importance due to associated environmental, anthropogenic and climatic impacts (Kalnay and Cai 2003). Urban estimates from Landsat data have been used within global biogeochemistry and climate models (Z. Zhu and Woodcock 2014), further scientific studies such as UHI investigations (Y. Hu et al. 2015) and targeted urban development policies (Schneider, Seto, and Webster 2005; Hepinstall-Cymerman, Coe, and Hutyra 2013). Whilst comparative studies (e.g. Li et al. 2014) have shown marginal holistic image accuracy difference between algorithm selection on per-pixel Landsat classification assuming sufficient training data. Traditional per-pixel methods, such as the maximum likelihood classifier (discussed in supplementary section 1), have been found to significantly over or underestimate urban area from Landsat data (Lu, Moran, and Hetrick 2011; Wu and Murray 2003). Addressing this error is important when accurate classifications are required for monitoring change in land use patterns whereby calculations of urban extent can influence decision-making (e.g. policy for sustainable urban development) (Schneider, Seto, and Webster 2005; Hepinstall-Cymerman, Coe, and Hutyra 2013; Miller and Small 2003; Bagan and Yamagata 2014).

Due to the heterogeneity of urban areas, sub-pixel classification methodologies have been increasingly applied to medium spatial resolution data to more accurately represent the mixture of land covers within a pixel (Lu, Moran, and Hetrick 2011; Lu and Weng 2006; Powell and Roberts 2008; F. Weng and Pu 2013; Wang et al. 2013). This has been achieved through variations of Spectral Mixture Analysis (SMA) where a set number of representative endmembers, frequently following the Vegetation, Impervious and Soil (V-I-S) framework, are used to model the entire image based on their spectral characteristics (Powell et al. 2007; Ridd 1995). However, endmembers may not fully represent image spectral variability or a pixel may be modelled by endmembers that do not represent materials within its field of view resulting in an inability to adequately portray the high spectral heterogeneity of the urban landscape (Powell et al. 2007). Support Vector Machine (SVM) spectral unmixing attempts to resolve this issue through consideration of a large number of training pixels which provides preferential accuracy in comparison to SMA although high dimensional data and large training samples can hinder its performance (Wang et al. 2013).

Comparatively the novel sub and hard pixel Import Vector Machine (IVM) classifier permits simultaneous multi-class comparison whilst continuously testing training samples for validity providing a more accurate solution (Roscher, Förstner, and Waske 2012). IVM has been found to consistently outperform decision trees, artificial neural networks and maximum likelihood algorithms (Watanachaturaporn, Arora, and Varshney 2008; Kotsiantis, Zaharakis, and Pintelas 2006; Huang, Davis, and Townshend 2002), with preferential (Braun, Weidner, and Hinz 2012) and comparable results to SVM (Roscher, Waske, and Forstner 2010). However, due to the heterogeneity of urban areas it is important to calibrate these sub-pixel approaches against high spatial resolution data that capture the diverse characteristics found within

urban environments (Lu, Moran, and Hetrick 2011). Perth, Western Australia (WA) is characterised by extensive urban diversity, surpassing all other major Australian and United States cities in terms of suburban development (Kelly, Weidmann, and Walsh 2011; U.S. Department of Commerce 2013). It therefore provides a suitable case study for assessing the ability of Landsat to map urban development, which is a pre-requisite for appropriate policy incorporation. This paper describes an approach to map the urban extent of the Perth Metropolitan Region (PMR) using an IVM classifier applied to medium spatial resolution imagery. The impact of sub-pixel land cover heterogeneity is investigated by comparing the urban area estimates to those derived from very high spatial resolution (20cm) imagery. An innovative, spatially explicit correction to account for over (or under) estimation of urban area is derived which improves the urban land cover estimates from medium resolution imagery.

2. Study area

The Perth Metropolitan Region (PMR) (Figure 1), WA has experienced sustained urban development since the 21st century in response to a rapidly growing resource sector (Kennewell and Shaw 2008). The majority of recent urban growth within the PMR has transpired as outward low-density development resulting in a maximum population density of 3,662 people per square kilometre which is 33% and 24% lower than Melbourne (10,827) and Sydney (14,747) respectively (Western Australian Planning Commission 2015; ABS 2015). The notion of the 'Australian dream', depicted as detached living in a green suburb, is most pronounced in Perth (Western Australian Planning Commission 2013a). As a result 79% of the current housing is detached, compared to 62% in Sydney, 72% in Melbourne and a national average of 74% (Kelly, Weidmann, and Walsh 2011; Western Australian Planning Commission 2013b). Globally, Australia surpasses other developed countries in terms of detached suburban

living with England having 42% of housing as either detached or semi-detached (Department for Communities and Local Government 2015). Similarly only 64.2% of USA housing stock is detached, with Perth eclipsing all of the major 25 USA metropolitan areas in terms of detached housing (U.S. Department of Commerce 2013). Low population density and outward expansion witnessed in Perth has generated high demand for dispersed amenities and services in a non-strategic, "lot-by-lot fashion" (Dhakal 2014). Suburbanisation of this nature has been identified as unsustainable due to impacts on ecological systems (e.g. habitat fragmentation) and socio-economic issues (e.g. amenity provisioning costs), with accurate urban area identification essential for sustainable future planning and maximum resource efficiency, particularly in Perth owing to its globally high suburbanisation and distributed population (Western Australian Planning Commission 2013a).

[Insert Figure 1 here]

Therefore, the PMR provides a globally diverse range of urban characteristics (e.g. compact urban central business district, older residential areas and new suburban developments) facilitating broad dataset comparison opportunities between Landsat and high spatial resolution urban area estimates. The high spatial resolution data identifies the complexity of these suburban and urban areas, which is obscured in medium and coarse spatial resolution datasets. This permits the extraction of individual features such as buildings, roads and vegetation that compose the urban environment and which are represented as a spectrally mixed pixel in Landsat imagery (illustrated in Figure 2) (Myint et al. 2011).

[Insert Figure 2 here]

Definitive feature detection from high resolution data can assist in refining urban area estimates produced from moderate spatial resolution satellite imagery (Lu, Moran, and Hetrick 2011; Wu and Murray 2003). More accurate satellite derived urban area estimates are imperative for ensuring appropriate data use for policy and environmental variable applications in order to mitigate the consequences of unsustainable urban development. This aligns with the criteria of effective land use planning within the City Resilience Framework (CRF) which is designed to improve city resilience (ARUP and The Rockefeller Foundation 2015).

3. Data

3.1. Landsat data

Cloud free Landsat scenes were obtained for 2007 from Landsat 5 Thematic Mapper (TM), coinciding with high resolution orthophotos (described in Section 3.2). Imagery were acquired within winter months (July path 113 and October path 112) corresponding with peak vegetation green-up which limits issues concerning the spectral separation between senescent vegetation, bare earth and some impervious surfaces (Feyisa et al. 2016; Chen et al. 2014). Landsat imagery was processed to standard terrain correction (Level 1T), geometrically and topographically corrected using Ground Control Points (GCPs) and a Digital Elevation Model (DEM) from the Global Land Survey 2000 dataset (Hansen and Loveland 2012). Landsat 5 TM surface reflectance values were derived from the Landsat Ecosystem Disturbance Adaptive Processing System (LEDPAS) (Hansen and Loveland 2012; Jeffrey G Masek et al. 2006) which corrects for atmospheric effects using the Second Simulation of a Satellite

Signal in the Solar Spectrum (6S) radiative transfer model (Vermote et al. 1997).

3.2. High spatial resolution airborne imagery

Radiometrically calibrated multispectral red (0.58-0.77 µm), green (0.48-0.63 µm), blue (0.41 µm -0.54 µm) and near-infrared (0.69-1.0 µm) orthophotos were acquired over 19 cloud free days commencing on 14 March (2007) as part of the Perth and Peel Urban Monitor Programme (Caccetta et al. 2012). Aerial imagery, obtained between 10am and 2pm to reduce shadow effects, were captured using a Microsoft UltraCAM-D at a height of 1300m resulting in a spatial resolution of 20 cm. Forward and side frame overlap of 60% and 30% respectively permitted automatic Digital Surface Model (DSM) extraction using geometric control points provided by WA's land information authority (Landgate). Extraction of ground points exclusively representing terrain variations facilitated derivation of a Ground Elevation Model (GEM) which, when subtracted from the DSM, generated a Relative Elevation Model (REM), depicting elevation relative to ground points.

Spatial and temporal inconsistencies in reflectance can arise from atmospheric scattering and absorption; instrument noise and Bidirectional Reflection Distribution Function (BRDF) effects. The latter describes the systematic variation in reflectance across an image due to differences in view and illumination angles and which is dependent on the surface 3D structure (Collings, Caccetta, and Campbell 2011). The orthophotos were provided as a surface reflectance product, corrected for multiplicative and additive errors over frames (e.g. instrument noise and atmospheric effects) and within frame viewing and illumination geometry (Caccetta et al. 2012; Collings, Caccetta, and Campbell 2011). Image pre-processing consisted of two steps. Firstly, a combined BRDF and atmospheric correction procedure was applied to retrieve surface reflectance for each image acquisition. Linear BRDF model parameters from the Li

Sparse reciprocal kernel (Wanner, Li, and Strahler 1995) were used to correct for BRDF effects. Atmospheric perturbations were corrected by assuming that the obtained digital number represented the relative reflectance affected by spatially dependent multiplicative and additive terms. These combined steps generated an internally consistent mosaicked dataset. 'True' surface reflectance was estimated through fitting global offset and gain values to replicate laboratory measured calibration targets based on the assumption that relative reflectance requires a linear transformation to true reflectance (Collings, Caccetta, and Campbell 2011).

4. Methodology

4.1. Landsat pre-processing

The two Landsat scenes covering the study area were combined to form a seamless image mosaic following the methodology of Pan et al. (2009). Voroni diagrams were created on the bisector between images with adjacent edges defined as seamlines, identifying effective mosaic polygons that specify pixels from each image to include in the final mosaic, facilitating less visible boundaries through blending of overlapping pixels (Pan et al. 2009) (Figure 1). Due to remaining residual noise in the mosaicked imagery caused by factors such as the brightening effect of thin clouds and atmospheric correction differences, surface reflectance values were standardised following the approach identified by Sexton et al. (2013):

$$p_{\mathrm{i,b}} = \frac{p_{\mathrm{x,b}}}{\max_{\mathrm{b}}} \tag{1}$$

where $p_{\mathrm{i,b}}$ is the standardised pixel value i, from band b based on the original surface reflectance x, standardised through division by a waveband specific upper reflectance limit which are: 0.1 (blue; 0.48μm), 0.11 (green; 0.56μm), 0.12 (red;

0.66µm), 0.225 (near-infrared; 0.84µm), 0.205 (shortwave-infrared; 1.65µm), 0.150 (shortwave-infrared 2; 2.22µm). The standardised values ($p_{\mathrm{i,b}}$) were then normalised against the summed band standardised values:

$$p_{\mathrm{j,b}} = \frac{p_{\mathrm{i,b}}}{\sum_{\mathrm{i}} p_{\mathrm{i,b}}} \quad (2)$$

where $\sum_{\mathrm{i}} p_{\mathrm{i,b}}$ is the sum of each standardised pixel across all bands (Sexton et al. 2013). This approach has been found to satisfactorily reduce variations generated from inherent residual noise across mosaicked imagery, for example due to differences in modelled atmospheric parameters within the LEDAPS algorithm (Sexton et al. 2013; Luo et al. 2014) (

Figure 3). Statistical assessment of image radiometric normalisation provided in MacLachlan et al. (2017a) found that the post-processed Landsat data exhibited significantly lower inter and intra Coefficient of Variation (CV) when compared to the pre-processed data.

[Insert Figure 3 here]

4.2. Landsat classification

The 2007 Landsat data was classified as a time series of data for seven sequential periods between 1990 and 2015 using an Import Vector Machine (IVM) classifier produced in MacLachlan et al. (2017a). The method uses a hybrid strategy which assesses whether new samples (termed import vectors) can be removed in each forward step in order to provide a smoother decision boundary which ideally leads to a more accurate solution (Roscher, Förstner, and Waske 2012). Samples are selected based on

how much their incorporation decreases the objective function to minimise the decision boundary to form the optimal separating hyperplane between overlapping clusters (e.g. land cover types) in spectral feature space (Mountrakis, Im, and Ogole 2011; Roscher, Förstner, and Waske 2012; J. Zhu and Hastie 2005). IVM generates two outputs: a soft (sub-pixel) dataset which defines the probability of a pixel containing a given classification value (e.g. land cover type) and a traditional 'hardened' classified dataset (Braun, Weidner, and Hinz 2012). Training samples were collected from the 2005 July Landsat 5 TM image, coinciding with peak vegetation greenness which provides the greatest spectral separability between vegetated and non-vegetated surfaces (Feyisa et al. 2016; Chen et al. 2014). Six land cover types were defined based on existing literature (e.g. X. Hu and Weng 2009; Schneider 2012; Feyisa et al. 2016) and scene analysis which are high reflectance urban (e.g. concrete), low reflectance urban (e.g. asphalt), forest, water, grassland and bare earth. Two urban land cover classes are specified to reduce spectral confusion between spectrally similarly classes (e.g. urban and bare earth) (X. Hu and Weng 2009). For each land cover type, 250 pixels were randomly identified from across the image for training the IVM classifier which follows the approach used by Foody and Mather (2006) and Pal and Mather (2003). The IVM algorithm is parameterised using the training data that generates a classification model consisting of spectral profiles for each land cover type, which are then matched to the Landsat mosaic during classification.

The resulting per-pixel (hardened) classification indicates that the total urban extent of the PMR has increased 45% (sub-pixel estimate of 33%) between 1990 (hardened estimate 706.88 km^2, sub-pixel estimate 736.93 km^2) and 2015 (hardened estimate 1027.22 km^2, sub-pixel estimate 979.84 km^2) (MacLachlan et al. 2017a). This can be broken down into low reflectance urban cover expanding from a hardened value

of 592.83 km^2 (sub-pixel estimate 668.46 km^2) to 839.00 km^2 (sub-pixel estimate 850.87 km^2) and high reflectance urban cover increasing from a hardened value of 114.05 km^2 (sub-pixel estimate 135.32 km^2) to 188.20 km^2 (sub-pixel estimate 214.06 km^2) across the same temporal period.

4.3. Google Earth Landsat accuracy assessment

Google Earth imagery consistent with the Landsat acquisition date was used to assess the accuracy of the hardened Landsat classification following previously published methods (e.g. Dorais and Cardille 2011; Cunningham et al. 2015; Song et al. 2016; Sun et al. 2015; Bagan and Yamagata 2014; Z. Zhu and Woodcock 2014). Using the Google Earth imagery, 300 random locations (50 per land cover class) within the PMR which were visually identified and compared to the classified land cover data, consistent with recommended land cover accuracy sample size of Congalton (2001) (Song et al. 2016). The 2007 Landsat classification obtained an accuracy of 84% and a Kappa Coefficient of 0.78. Urban land cover estimates had a producer's accuracy of 83% and user's accuracy of 87.37%. MacLachlan et al. (2017a) provide a full breakdown of urban temporal change and associated accuracy for all imagery in the Landsat timeseries (1990-2015), with the Landsat classification data available from the pangea open access publisher (DOI: 10.1594/PANGAEA.871017) (MacLachlan et al. 2017b).

4.4. Aerial image classification

Urban areas are complex, heterogeneous environments which are challenging to classify even when using high spatial resolution multi-spectral imagery (Varshney and Rajesh 2014; Lu, Moran, and Hetrick 2011). Within urban areas, traditional moderate and coarse spatial resolution pixel based classification methods present multiple challenges due to the land surface spatial heterogeneity and the spectral similarity between urban

and non-urban materials (Myint et al. 2011). To characterise the influence of spatial resolution on the ability to map urban areas, high spatial resolution multispectral ortho-imagery (20 cm) were classified into the four broad land cover types. To reduce data processing requirements, four 3 km^2 subsets were chosen that are representative of the land cover composition and spatial heterogeneity found within Perth (Figure 1). These subsets are an out of town development area (East Beechboro), the Central Business District (CBD), an older suburban area (Palmrya, Melville) and a largely vegetated region (Keysbrook). Using the high spatial resolution multispectral imagery and a relative elevation model, an Object Based Image Analysis (OBIA) method was applied to classify each subset into vegetation, urban, bare earth and water (Figure 3). OBIA methods are often applied to high spatial resolution imagery as they include spatial, textural and spectral information to classify the scene (Myint et al. 2011). Incorporating surface elevation measurements into urban classifications has been found to improve building (urban) extraction accuracy (Aguilar et al. 2012; Poznanska, Bayer, and Bucher 2013). Surface elevation estimates and Normalised Difference Vegetation Index (NDVI) data provided additional urban classification parameters, with refinement (e.g. additions and alterations) made based on object spatial, spectral and textural properties. Unlike the Landsat imagery, the airborne imagery were collected during the late dry season when the grass was senescent which resulted in textural and spectral similarity between bare earth and roads. To mitigate the impact of potential misclassification between these features, Landgate road and, where appropriate, rail vector dataset was used for identification of coincident image objects for urban assignment.

[Insert Table 1 here]

4.5. Dataset comparison and Landsat refinement

In order to compare the orthophoto and Landsat land cover classifications, the two urban (high and low reflectance) and two vegetation (woodland and grassland) Landsat land cover classes were merged so that both land cover classifications contained four identical classes. To facilitate comparison between the high spatial resolution orthophoto-derived classification and the Landsat classification, the orthophoto land cover data is aggregated to Landsat spatial resolution to provide a 'soft' and a 'hard' land cover dataset. To create the soft 30 m^2 orthophoto-derived classification, each resampled 30 m^2 pixel area contains the proportion of each land cover type within it (Lu, Moran, and Hetrick 2011) (Figure 3b). This dataset was subsequently 'hardened' by assigning the pixel land cover type according to the dominant land cover found within the 30 m^2 area.

The comparison methodology is to firstly compare the per-pixel (i.e. hardened) Landsat land cover classification with the aggregated (30 m^2) orthoimage classification. Mis-classified Landsat pixels are assessed further to establish the conditions that lead to erroneous classification using the sub-pixel proportion information (i.e. soft classification datasets). The latter are also used to identify a spatially explicit correction model to improve urban area estimates from moderate spatial resolution imagery.

5. Results

5.1. Orthophoto and Landsat land cover comparison

A comparison is conducted between the orthophoto land cover classification, aggregated to 30 m^2 spatial resolution using the majority land cover, and the IVM 'hardened' Landsat classification. At its native spatial resolution (20 cm; Figure 4*a*-*d*(i)), the orthophoto land cover classification (Figure 4*a*-*d*(ii)) captures the land cover

spatial heterogeneity found within each region and highlights the difference in the spatial structure between these regions.

[Insert Figure 4 here]

A comparison is carried out between the orthophoto land cover classification, aggregated to 30 m^2 spatial resolution, and the 'hardened' Landsat classification. Figure 4(iii) illustrates the spatial agreement between these datasets and highlights those pixels where the same land cover type (true) has been assigned to a pixel in both classifications. The areas which are more homogeneous at Landsat's spatial resolution, such as the CBD (urban, Figure 4*b*) and Keysbrook (vegetation, Figure 4*d*), have greater level of agreement (73.14% and 95.68% respectively). In contrast, the more heterogeneous subsets (East Beechboro and Palmrya, Figure 4*a* and *c*), have much lower levels of agreement (56% and 32% respectively). The differences in agreement result from the sub-pixel heterogeneity at 30 m^2 spatial resolution. Table 2 shows the percentage of Landsat pixels which contain >50% of a given land cover for each subset region.

[Insert Table 2 here]

To investigate the influence of sub-pixel heterogeneity on the ability of Landsat to identify the pixel land cover type, the classification accuracy is determined as a function of the percentage of urban area within each Landsat pixel for all four subsets (Figure 5). The urban percentage cover within each Landsat pixel is derived from the orthophoto land cover classification which has been aggregated to 30 m^2 and which

provides the proportion of each land cover within each pixel. The accuracy of the hardened Landsat classification was determined through comparison against the 'hardened' (e.g. aggregated to $30m^2$) orthophoto land cover classification where the per-pixel land cover type was determined based on the land cover type with the greatest sub-pixel proportion. Figure 5 indicates that the hardened Landsat classification results in a relatively high accuracy, with an average of 85.4% (excluding Keysbrook), for pixels containing >50% urban land cover (according to the high spatial resolution land cover classification). In the subsets of East Beechboro, the CBD and Palmrya, the overall Landsat classification accuracy drastically declines to 3.5-6.2% when urban land cover within a 30 m^2 pixel area decreases to 40-50%. The classification accuracy then increases with decreasing sub-pixel urban cover which is particularly evident with Landsat pixels containing 0-10% urban cover. Keysbrook, on the other hand, is a largely vegetated region and exhibits lower accuracy with increasing urban land cover.

[Insert Figure 5 here]

In order to understand the counter-intuitive behaviour of such as rapid decrease in classification accuracy in pixels which contain ~40-50% urban area (Figure 5), an analysis of the percentage of pixels classified as a given land cover type is presented. To do so, all pixels containing different ranges in urban percentage cover (e.g. 0-10%, 20-30% etc) were identified using the high spatial resolution land cover dataset. The total percentage of each land cover type was calculated for all pixels that contained urban percentage cover within each range urban percentage cover (e.g. 0-10%, 20-30% etc) using hardened IVM Landsat land cover dataset and the aggregated high spatial

resolution land cover dataset (i.e. defined by the dominant land cover type within a 30 m^2 pixel area).

Figure 6 illustrates the percentage of pixels identified as a given land cover type as indicated by the hardened Landsat land cover dataset and the hardened high spatial resolution orthophoto land cover dataset for pixels which contain differing percentage urban cover (e.g. 0-10%) derived using the original high spatial resolution orthophoto land cover classification for the East Beechboro subset. This area was selected as it is an intermediate area in terms of land cover heterogeneity (Figure 2 and 4). The results indicate that the hardened Landsat classification consistently overestimates urban land cover when compared to the 'hardened' high spatial resolution classification which has been aggregated to 30 m^2 based on the dominate land cover within the Landsat pixel area for pixels with 10-50% urban defined by high resolution data. Table 3 and Figure 7 illustrates the sub-pixel (30 m^2) percentage urban land cover for East Beechboro with the original reflectance imagery for this area shown in Figure 2. The hardened high spatial resolution land cover dataset (left bar in each plot (Figure 6)) indicates that pixels containing <50% urban land cover are largely dominated by vegetation. In contrast, Landsat largely identifies these pixels as being either urban or vegetated to differing extents and more correctly identifies pixels with 0-10% urban land cover as being predominantly vegetated. For example, pixels containing 40-50% urban area are correctly identified as being vegetated (98.4% of pixels within this range) by the hardened high spatial resolution land cover dataset since these pixels contain on average 54.72% vegetation, 44.83% urban and 0.45% bare earth. In contrast, the hardened Landsat land cover dataset identifies 5.7% of pixels containing 40-50% urban cover as being vegetation, 74.3% being urban and 20.1% being bare earth. As the percentage of urban land cover decreases, the overall accuracy of the hardened Landsat classification

increases due to the increase in Landsat vegetation cover which increases from 5.7% (40-50% urban cover) to 75.4% (0-10% urban cover). The results are similar for the other regional subsets. The rapid decrease in accuracy between 40-50% and 50-60% (Figure 5) appears extreme as the subset regions are dominated by vegetation and urban land cover (Table 1) which results in the aggregated 30 m^2 pixels being assigned to vegetation when the percentage urban cover is <50% or urban when the percentage urban cover is >50% (Figure 6).

[Insert Figure 6 here]

[Insert Table 3 here]

[Insert Figure 7 here]

The results in Figure 6 suggest that the spectral data used to train the IVM classification (discussed in section 4.2) contained spectrally 'mixed' pixels resulting in land cover type misclassification. To investigate this, the spectral reflectance from Landsat pixels containing 20-30% urban cover for the Palmrya subset, which had the lowest overall agreement and which were identified as being mostly vegetated by the hardened high spatial resolution land cover dataset, are extracted and compared to the spectral reflectance profiles used to train the IVM classification algorithm. Figure 8 indicates that there are strong similarities between the average spectral reflectance profile used to train the IVM classification algorithm and the average spectral profile of the misclassified pixels. This suggests that the IVM classification algorithm is accurately representing the Landsat pixel spectral reflectance properties but that the

training data used to develop the classification model contained a high proportion of mixed pixels.

[Insert Figure 8 here]

Pure (i.e. homogeneous) pixels are conventionally selected to train classification models (e.g. F. Weng and Pu 2013) but these are inherently difficult to identify in urban areas owing to the multitude of land covers within a Landsat pixel area. Using the high spatial resolution classification, the percentage of pure pixels, defined here as those containing between 90-100% of a single land cover type, were identified (Table 4). It is evident that some regions contain a high percentage of pure pixels for a given land cover type, such as vegetation in Keysbrook (92%), but that other land cover types within a region typically have much lower percentages of pure pixels. Pure urban pixels are particularly limited in all subset regions. Whilst the CBD subset obtains a high percentage of pure urban pixels (28%) these are predominately urban areas with high spectral reflectance (e.g. concrete), differing from subsets with urban areas which have urban areas with both high and low spectral reflectance (e.g. East Beechboro; Figure 2).

[Insert Table 4 here]

5.2. Comparison between Landsat and high spatial resolution impervious surface estimates

Landsat data have been widely applied to map impervious surface area in order to assess its effects on: urban growth dynamics (J. G. Masek, Lindsay, and Goward 2000), the UHI effect (Y. Hu et al. 2015) and surface run-off (Q. Weng 2001). Figure 6 indicates that the ‘hardened’ Landsat IVM classification overestimates urban land

cover, particularly for pixels containing <50% urban area. The IVM classifier also provides a 'soft' land cover dataset that quantifies the sub-pixel land cover proportions.

Here we investigate the utility of the sub-pixel Landsat urban land cover estimates by comparing them to those derived from the high spatial resolution land cover dataset (20 cm) which is used to provide the actual land cover proportion within each 30 m^2 pixel area. Urban area estimates from each of the four subsets (Figure 1) were spatially averaged over different size spatial windows (30×30 m, 90×90 m, 150×150 m and 210×210 m) in order to account for any errors resulting from pixel heterogeneity, spatial mis-registration, residual atmospheric and BRDF effects and phenological differences (Ju et al. 2012; Liang, Fang, and Chen 2001; Maiersperger et al. 2013; Ghimire, Rogan, and Miller 2010; Lu, Moran, and Hetrick 2011) that may increase the uncertainty in estimating land cover proportions (Sexton et al. 2013; Lu, Moran, and Hetrick 2011). Comparison of impervious surface proportions at 30 m^2, for example the CBD subset (Figure 9), reiterates the overestimation of urban area at 30 m^2 spatial resolution, with a clustering of values toward the upper percentage boundaries associated with lower urban area estimates from the high spatial resolution classification. When neighbourhood averaging is applied, the agreement in urban area typically improves with increasing window size although the subset specific bias remains consistent (Table 5). It is also evident that urban area is still overestimated with decreasing urban sub-pixel proportion even when utilising the sub-pixel IVM Landsat classification results.

[Insert Figure 9 here]

[Insert Table 5 here]

5.3. Refining Landsat estimations using high spatial resolution data

Sub-pixel land cover heterogeneity influences Landsat urban area overestimation which must be considered in order to reduce the bias and improve Landsat derived urban area estimation (Herold et al. 2002; Lu, Moran, and Hetrick 2011; Varshney and Rajesh 2014; Schneider 2012). The complexity and diversity of urban areas identified here from high spatial resolution data, with biases ranging from -2.4% to -34.67%, highlights the inappropriateness of applying a single model to adjust the moderate spatial resolution urban area estimates in a metropolitan region (e.g. Lu, Moran, and Hetrick 2011). The Landsat sub-pixel urban areas estimates from all four subsets were stratified based on the Landsat sub-pixel derived urban area and calibrated against the percentage of urban area from the high spatial resolution classification within each moderate spatial resolution pixel area. Both datasets were averaged at the neighbourhood level using a 210 x 210m window as this provided the best overall relationship (Table 5). Stratification of Landsat sub-pixel urban estimates into divisions of 10%, consistent with previous results, were selected to develop (using 50% of the data) and test (remaining 50% of the data) regression models to improve the dataset agreement (Lu, Moran, and Hetrick 2011).

The applied spatially explicit models reduced the bias and Root Mean Square Error (RMSE) between the predicted (moderate spatial resolution) and observed (high spatial resolution) estimates (Table 6). It is evident from Table 6 that the adjustment made to the Landsat urban area estimates reduced the overestimation difference of urban area by between 34.38% and 80.67%, with the largest improvement found within Keysbrook. Whilst the corrected Landsat urban area estimates still overestimates the urban area compared to the high spatial resolution dataset the corrected moderate spatial

resolution urban area reduces moderate resolution urban area over (under) estimation by on average 55.08% in comparison to the high spatial resolution dataset reducing the average overestimation from 11.86 km^2 per subset to just 0.09 km^2 (Table 6). In the case of this study area, this approach is appropriate for producing more accurate urban area statistics. Due to the frequently reported over and under estimation of land cover estimates by moderate spatial resolution data this approach can refine urban estimates for planning development policies that may inform decision makers (Z. Zhu and Woodcock 2014; Schneider, Seto, and Webster 2005; Hepinstall-Cymerman, Coe, and Hutyra 2013). However, the derived correction values are not globally applicable since the spatial structure and makeup of urban and suburban areas varies regionally, nationally and globally. Nevertheless the methodology implemented here could be replicated to produce localised correction values from other sources of high resolution imagery (e.g. digitisation of Google Earth imagery) to calibrate urban area estimates from moderate spatial resolution data.

[Insert Table 6 here]

6. Discussion

Refined urban estimates are vital in ensuring suitable sustainable and strategic planning decisions are implemented (Bettencourt and West 2010; Wu and Murray 2003). The hybrid spatial resolution approach applied here to estimate urban area was necessary due to the difficulty in accurately estimating urban area using a traditional per-pixel classification methods. This was due to a combination of the sensors moderate (30 m^2) spatial resolution, land surface heterogeneity and the selection of 'mixed' pixels for use in training the classification algorithm. The overall classification accuracy, determined

using Google Earth imagery, was on average 84%, which is similar to that found in other studies, albeit for different urban areas (e.g. Gislason, Benediktsson, and Sveinsson 2006; Bagan and Yamagata 2014; Sundarakumar et al. 2012; Luo et al. 2014).

Closer examination of the moderate spatial resolution classification results using a higher resolution dataset indicates that when urban land cover within a 30 m^2 area decreases to 40-50% (based on high spatial resolution classification) the Landsat classification accuracy decreased from 85.4% to between 3.5 and 6.2%. This resulted from the Landsat classification overestimating urban area in comparison to high spatial resolution data (Figure 5) which more correctly identified these pixels as containing a greater per-pixel proportion of vegetation. Pixels containing 40-50% urban cover, contained on average 54.50% vegetation cover excluding Keysbrook. The dominance of vegetation and urban land covers in the regional subset, when ascribed to a 30 m^2 pixel area based on the majority land cover, results in a rapid change in classification accuracy. Strong spectral similarities between training data and misclassified pixels (Figure 8) suggests that the spectral reflectance observations used to train the classification algorithm contained spectrally mixed pixels. The average percentage urban area within a moderate spatial resolution pixel area derived from the high resolution data was 16.56%, 65.66%, 42.21% and 0.90% for East Beechboro, CBD, Palmyra and Keysbrook respectively. The percentage of 'pure' pixels, defined as those containing over 90% urban land cover, was 28% for the CBD but <2.5% for the suburban regional subsets. This highlights the difficulty in selecting pure pixels at moderate spatial resolution and in accurately disentangling mixed spectral reflectance's without the aid of high spatial resolution data. Overestimation of urban extent was most prominent in Keysbrook, where vegetation dominates the subset (97.36%, Table 1). In

this instance, Landsat derived urban area corresponded to 0.28 km^2 compared to 0.08 km^2 from high spatial resolution classification; a difference of only 0.2 km^2 but which equates to 251.74%. In terms of total area difference, the East Beechboro and the CBD Landsat subsets were found to contain 1.75 km^2 and 1.7 km^2 more urbanised area, whilst Palmyra data overestimated urban area by 2.8 km^2 compared to the high spatial resolution equivalent due to its suburban nature and associated pixel heterogeneity (Figure 4).

Spatially averaging the Landsat and orthophoto land cover classifications, to account for potential errors in the datasets (Ghimire, Rogan, and Miller 2010), improved their relationship although Landsat still overestimated urban area with differing bias per subset. Over (under) estimation of urban land from Landsat estimations could result in an under (over) prediction on further environmental variables (e.g. UHI) or policy applications. Multiple studies have used classified per-pixel moderate spatial resolution data to influence policy changes through monitoring urban growth (e.g. Schneider, Seto, and Webster 2005; Hepinstall-Cymerman, Coe, and Hutyra 2013). However, per-pixel methodologies fail to address the issue of mixed pixels, which, as shown here, can result in overestimation of urban area (average: 126.14%, equivalent to 54.79 km^2 within the PMR) (Lu, Moran, and Hetrick 2011). Sub-pixel methods attempt to remedy this issue, but have been found to inaccurately separate impervious land cover from other land cover types resulting in poor representation of impervious surface area (Lu, Moran, and Hetrick 2011). Consequently over estimation of urban area may have resulted in sub-optimal policies that fail to maximise resource and amenity efficiency (Turner, Lambin, and Reenberg 2010; Downs 2005).

Calibrating Landsat urban estimates using high spatial resolution data reduces the bias, RMSE and improves urban area estimation. However, the range of bias values

across subsets of differing urban land cover characteristic highlights the inappropriateness of a single regression model due to pixel heterogeneity influencing overestimation (Lu, Moran, and Hetrick 2011). Spatially explicit models, as presented here, permit varying moderate spatial resolution refinement by considering the influence of surface heterogeneity. Whilst the limited availability of low cost high spatial resolution data can preclude analysis of this type, subset digitisation of Google Earth or unmanned aerial vehicle (UAV) imagery may provide a suitable alternative for calibrating Landsat data for improved urban area estimates. Enhanced estimates of urban area would facilitate planning policies which avoid potential environmental and socio-economic consequences of urban development than can result from policies based on over (or under) predicted urban area (ARUP and The Rockefeller Foundation 2015). For example, classified Landsat data was used to identify spatial clustering, peri urban development and specialisation of land use in Chengdu, Sichuan province not considered by China's original 1990 Go West policy, aimed at economically boosting the West of the country. Results were used to reform policy and remediate issues of urban management including: service, infrastructure and resource deficiencies (Schneider, Seto, and Webster 2005). However, traditional Landsat classification may over (or under) estimate urban area and result in ineffective planning, environmental and policy decisions (Miller and Small 2003; Pravitasari et al. 2015). Therefore classified sub-pixel data alongside high spatial resolution imagery (e.g. UAV, Google Earth, high spatial resolution aerial or satellite imagery) as presented here can refine urban estimates facilitating improved decision making whilst maximising often limited financial resources. This is especially important in developing countries in regards to directing urban development and resources based on factors including: poverty,

environmental hazards (e.g. flooding) and current amenity centres (Marfai, Sekaranom, and Ward 2014; Suryahadi and Sumarto 2003).

7. Conclusion

Landsat imagery from 2007 was used to map the urban extent within the Perth Metropolitan Region (PMR) using an Import Vector Machine (IVM) classifier which provides both a per-pixel and a sub-pixel classified datasets. The 2007 Landsat classification overall average accuracy was 84% with associated Kappa coefficient of 0.78. Comparison between the Landsat per-pixel urban area and urban area estimates obtained from a high spatial resolution (20 cm) orthophoto-derived classification indicates that the moderate spatial resolution classification overestimates urban extent by 126.14 % on average, which is equivalent to 54.79 km^2 in the study area. Similarly, when the high spatial resolution urban area estimates are compared to those derived using a sub-pixel Landsat classification, the latter still overestimates urban extent by 120%.

Accurately quantifying urban expansion within the PMR due to the large population growth over the last decade is important in order to make the efficient use of current resources and to avoid additional amenity, environmental and health expenditure that can impact sprawling cities. Landsat data provides the longest time series of medium spatial resolution imagery to map and monitor urban area. However, the reported over and underestimation inhibits accurate quantification of urbanised land cover which increases uncertainty within global climate models, environmental studies and targeted urban planning policy. Neighbourhood averaging, to account for potential errors in the datasets, improved the agreement between the two datasets but Landsat sub-pixel overestimation still remained. The broad differences in bias between the difference subsets indicates that a single regression model is inappropriate to

heterogeneous urban land cover estimates. Therefore, the moderate spatial resolution urban area estimates were corrected using spatially explicit regression models which, on average, across the four subsets reduced the bias and Root Mean Square Error (RMSE) by 17.02 km^2 and 6.65 km^2 respectively, whilst reducing moderate resolution urban area over (under) estimation by 55.08%

Current and future Earth Observation (EO) satellites that provide complimentary data with enhanced spatial, spectral and temporal resolution, such as Sentinel-2, may further reduce over or under estimation of urban area experienced by moderate spatial resolution sensors such as Landsat. Similarly, high spatial resolution satellite sensors, such as Worldview-3, are able to remediate discrepancies by capturing the fine spatial detail of urban environments but their cost and small swath limit their widespread application. This might change with companies, such as Planet, which are launching large numbers of small micro-satellites that provide high spatial resolution data more frequently. Accurate urban land cover and land use mapping is essential in understanding the impact of urban expansion on, for example, social-ecological systems and human-health and will improve future sustainable planning of our cities.

Supplementary Materials: Traditional classification detail is outlined in the supplementary documentation. The classified Landsat data reported in this paper are archived at the Pangea open access data publisher for earth and environmental science. DOI: 10.1594/PANGAEA.871017.

Geolocation Information: This research was conducted over the Perth Metropolitan Region, Western Australia, Australia, 31.9505° S, 115.8605° E.

Acknowledgments: This work was supported by the Economic and Social Research Council [grant number ES/J500161/1]. We would like to thank the World University Network (WUN) for facilitating institutional visits, the University of Western Australia for supplying high-resolution orthophotos of the Perth Metropolitan Region and the United States Geological Survey (USGS) for providing Landsat surface reflectance imagery.

Conflicts of Interest: The authors declare no conflict of interest and the founding sponsors had no role in the design of the study; in the collection, analyses, or interpretation of data; in the writing of the manuscript, and in the decision to publish the results.

References

ABS. 2015. *Australian National Accounts 1988-2015*. *Australian Bureau of Statistics*. Belconnen, ACT, Australia.

Aguilar, M a, R Vicente, F J Aguilar, A Fernández, and M.M Saldaña. 2012. "Optimizing Object-Based Classification in Urban Environments Using Very High Resolution Geoeye-1 Imagery." In *ISPRS Annals of the Photogrammetry, Remote Sensing and Spatial Information Sciences*, 1–7:99–104. doi:10.5194/isprsannals-I-7-99-2012.

Akbari, Hashem, Shea Rose, and Haider Taha. 2003. "Analyzing the Land Cover of an Urban Environment Using High-Resolution Orthophotos." *Landscape and Urban Planning* 63 (1): 1–14. doi:10.1016/S0169-2046(02)00165-2.

ARUP, and The Rockefeller Foundation. 2015. *City Resilience Framework—100 Resilient Cities*. *The Rockefeller Foundation*. New York, NY, USA.

Bagan, Hasi, and Yoshiki Yamagata. 2014. "Land-Cover Change Analysis in 50 Global Cities by Using a Combination of Landsat Data and Analysis of Grid Cells." *Environmental Research Letters* 9 (6). IOP Publishing: 64015. doi:10.1088/1748-9326/9/6/064015.

Bettencourt, Luis, and Geoffrey West. 2010. "A Unified Theory of Urban Living." *Nature* 467 (913): 9–10. doi:10.1038/467912a.

Braun, Andreas Ch, Uwe Weidner, and Stefan Hinz. 2012. "Classification in High-

Dimensional Feature Spaces-Assessment Using SVM, IVM and RVM with Focus on Simulated EnMAP Data." *IEEE Journal of Selected Topics in Applied Earth Observations and Remote Sensing* 5 (2): 436–443. doi:10.1109/JSTARS.2012.2190266.

Caccetta, Peter, Simon Collings, Andrew Devereux, Kass Hingee, Don Mcfarlane, Anthony Traylen, and Xiaoliang Wu. 2012. *Urban Monitor : Enabling Effective Monitoring and Management of Urban and Coastal Environments Using Digital Aerial Photography Final Report – Transformation of Aerial Photography into Digital Raster Information Products*. CSIRO, Australia.

Cai, Yuanbin, Hao Zhang, Peng Zheng, and Wenbin Pan. 2016. "Quantifying the Impact of Land use/Land Cover Changes on the Urban Heat Island: A Case Study of the Natural Wetlands Distribution Area of Fuzhou City, China." *Wetlands*. doi:10.1007/s13157-016-0738-7.

Chen, T., R. A M de Jeu, Y. Y. Liu, G. R. van der Werf, and A. J. Dolman. 2014. "Using Satellite Based Soil Moisture to Quantify the Water Driven Variability in NDVI: A Case Study over Mainland Australia." *Remote Sensing of Environment* 140: 330–338. doi:10.1016/j.rse.2013.08.022.

Collings, S., P. Caccetta, and N. Campbell. 2011. "Empirical Models for Radiometric Calibration of Digital Aerial Frame Mosaics." *IEEE Transactions on Geoscience and Remote Sensing* 49 (7): 2573–2588. doi:10.1109/TGRS.2011.2108301.

Congalton, Russell G. 2001. "Accuracy Assessment and Validation of Remotely Sensed and Other Spatial Information." *International Journal of Wildland Fire* 10: 321–328. doi:10.1071/WF01031.

Cunningham, Sean, John Rogan, Deborah Martin, Verna DeLauer, Stephen McCauley, and Andrew Shatz. 2015. “Mapping Land Development through Periods of Economic Bubble and Bust in Massachusetts Using Landsat Time Series Data.” *GIScience & Remote Sensing* 1603 (2016). doi:10.1080/15481603.2015.1045277.

Department for Communities and Local Government. 2015. *English Housing Survey: Housing Stock Report, 2014-2015*. *English Housing Survey*. London, UK. doi:10.1017/CBO9781107415324.004.

Dhakal, Subas P. 2014. “Glimpses of Sustainability in Perth , Western Australia : Capturing and Communicating the Adaptive Capacity of an Activist Group.” *Consilience: The Jounral of Sustainable Development* 11 (1): 167–182.

Dorais, Alexis, and Jeffrey Cardille. 2011. “Strategies for Incorporating High-Resolution Google Earth Databases to Guide and Validate Classifications: Understanding Deforestation in Borneo.” *Remote Sensing* 3 (6): 1157–1176. doi:10.3390/rs3061157.

Downs, Anthony. 2005. “Smart Growth: Why We Discuss It More than We Do It.” *Journal of the American Planning Association* 71 (4): 367–378. doi:10.1080/01944360508976707.

Feyisa, Gudina L., Henrik Meilby, G. Darrel Jenerette, and Stephan Pauliet. 2016. “Locally Optimized Separability Enhancement Indices for Urban Land Cover Mapping: Exploring Thermal Environmental Consequences of Rapid Urbanization in Addis Ababa, Ethiopia.” *Remote Sensing of Environment* 175: 14–31. doi:10.1016/j.rse.2015.12.026.

Foody, Giles M., and Ajay Mathur. 2006. “The Use of Small Training Sets Containing

Mixed Pixels for Accurate Hard Image Classification: Training on Mixed Spectral Responses for Classification by a SVM." *Remote Sensing of Environment* 103 (2): 179–189. doi:10.1016/j.rse.2006.04.001.

Friedl, M.A, D.K McIver, J.C.F Hodges, X.Y Zhang, D Muchoney, A.H Strahler, C.E Woodcock, et al. 2002. "Global Land Cover Mapping from MODIS: Algorithms and Early Results." *Remote Sensing of Environment* 83 (1–2): 287–302. doi:10.1016/S0034-4257(02)00078-0.

Ghimire, B., J. Rogan, and J. Miller. 2010. "Contextual Land-Cover Classification: Incorporating Spatial Dependence in Land-Cover Classification Models Using Random Forests and the Getis Statistic." *Remote Sensing Letters* 1 (1): 45–54. doi:10.1080/01431160903252327.

Gislason, Pall Oskar, Jon Atli Benediktsson, and Johannes R. Sveinsson. 2006. "Random Forests for Land Cover Classification." *Pattern Recognition Letters* 27 (4): 294–300. doi:10.1016/j.patrec.2005.08.011.

Hansen, Matthew C., and Thomas R. Loveland. 2012. "A Review of Large Area Monitoring of Land Cover Change Using Landsat Data." *Remote Sensing of Environment* 122: 66–74. doi:10.1016/j.rse.2011.08.024.

Hepinstall-Cymerman, Jeffrey, Stephan Coe, and Lucy R. Hutyra. 2013. "Urban Growth Patterns and Growth Management Boundaries in the Central Puget Sound, Washington, 1986-2007." *Urban Ecosystems* 16 (1): 109–129. doi:10.1007/s11252-011-0206-3.

Herold, Martin, Meg Gardner, Brian Hadley, and Dar Roberts. 2002. "The Spectral Dimension in Urban Land Cover Mapping from High-Resolution Optical Remote

Sensing Data." *Symposium A Quarterly Journal In Modern Foreign Literatures* 6: 1–8. doi:10.1109/TGRS.2003.815238.

Howard, Luke. 1988. *The Climate of London*. London, UK: Cambridge University Press.

Hu, Leiqiu, and Nathaniel a Brunsell. 2015. "Remote Sensing of Environment A New Perspective to Assess the Urban Heat Island through Remotely Sensed Atmospheric pro Fi Les." *Remote Sensing of Environment* 158: 393–406. doi:10.1016/j.rse.2014.10.022.

Hu, Xuefei, and Qihao Weng. 2009. "Estimating Impervious Surfaces from Medium Spatial Resolution Imagery Using the Self-Organizing Map and Multi-Layer Perceptron Neural Networks." *Remote Sensing of Environment* 113 (10): 2089–2102. doi:10.1016/j.rse.2009.05.014.

Hu, Yonghong, Gensuo Jia, Meiting Hou, Xiaoxuan Zhang, Feixiang Zheng, and Yonghe Liu. 2015. "The Cumulative Effects of Urban Expansion on Land Surface Temperatures in Metropolitan Jingjintang, China Yonghong." *Journal of Geophysical Research: Atmospheres RESEARCH*, 9932–9943. doi:10.1002/2014JD022994.Received.

Huang, C., L. S. Davis, and J. R. G. Townshend. 2002. "An Assessment of Support Vector Machines for Land Cover Classification." *International Journal of Remote Sensing* 23 (4): 725–749. doi:10.1080/01431160110040323.

Imhoff, Marc L., William T. Lawrence, David C. Stutzer, and Christopher D. Elvidge. 1997. "A Technique for Using Composite DMSP/OLS 'City Lights' Satellite Data to Map Urban Area." *Remote Sensing of Environment* 61 (3): 361–370.

doi:10.1016/S0034-4257(97)00046-1.

Ju, Junchang, David P. Roy, Eric Vermote, Jeffrey Masek, and Valeriy Kovalskyy. 2012. “Continental-Scale Validation of MODIS-Based and LEDAPS Landsat ETM+ Atmospheric Correction Methods.” *Remote Sensing of Environment* 122: 175–184. doi:10.1016/j.rse.2011.12.025.

Kalnay, Eugenia, and Ming Cai. 2003. “Impact of Urbanization and Land-Use Change on Climate.” *Nature* 423: 528–531. doi:10.1038/nature01649.1.

Kelly, J. F., B. Weidmann, and M. Walsh. 2011. *The Housing We’d Choose*. *Grattan Institue*. Melbourne, Australia.

Kennewell, Catherine, and Brian J. Shaw. 2008. “Perth, Western Australia.” *Cities* 25 (4): 243–255. doi:10.1016/j.cities.2008.01.002.

Kotsiantis, S. B., I. D. Zaharakis, and P. E. Pintelas. 2006. “Machine Learning: A Review of Classification and Combining Techniques.” *Artificial Intelligence Review* 26 (3): 159–190. doi:10.1007/s10462-007-9052-3.

Li, Congcong, Jie Wang, Lei Wang, Luanyun Hu, and Peng Gong. 2014. “Comparison of Classification Algorithms and Training Sample Sizes in Urban Land Classification with Landsat Thematic Mapper Imagery.” *Remote Sensing* 6 (2): 964–983. doi:10.3390/rs6020964.

Liang, S., H. Fang, and M. Chen. 2001. “Atmospheric Correction of Landsat ETM+ Land Surface Imagery. I.\nMethods.” *IEEE Transactions on Geoscience and Remote Sensing* 39 (11): 2490–2498. doi:10.1109/36.964986.

Lu, Dengsheng, Guiying Li, Wenhui Kuang, and Emilio Moran. 2014. “Methods to

Extract Impervious Surface Areas from Satellite Images." *International Journal of Digital Earth* 7 (2015): 93–112. doi:10.1080/17538947.2013.866173.

Lu, Dengsheng, Emilio Moran, and Scott Hetrick. 2011. "Detection of Impervious Surface Change with Multitemporal Landsat Images in an Urban-Rural Frontier." *ISPRS Journal of Photogrammetry and Remote Sensing : Official Publication of the International Society for Photogrammetry and Remote Sensing (ISPRS)* 66 (3): 298–306. doi:10.1016/j.isprsjprs.2010.10.010.

Lu, Dengsheng, and Qihao Weng. 2006. "Use of Impervious Surface in Urban Land-Use Classification." *Remote Sensing of Environment* 102 (1–2): 146–160. doi:10.1016/j.rse.2006.02.010.

Luo, Jieqiong, Peijun Du, Samat Alim, Xiangjian Xie, and Zhaohui Xue. 2014. "Annual Landsat Analysis of Urban Growth of Nanjing City from 1980 to 2013." *2014 Third International Workshop on Earth Observation and Remote Sensing Applications (EORSA)*, 357–361. doi:10.1109/EORSA.2014.6927912.

MacLachlan, Andrew, Eloise Biggs, Gareth Roberts, and Bryan Boruff. 2017a. "Urban Growth Dynamics in Perth, Western Australia: Using Applied Remote Sensing for Sustainable Future Planning." *Land* 6 (1): 9. doi:10.3390/land6010009.

MacLachlan, Andrew, Eloise Biggs, Gareth Roberts, and Bryan Boruff. 2017b. "Classified Earth Observation Data between 1990 and 2015 for the Perth Metropolitan Region, Western Australia Using the Import Vector Machine Algorithm." PANGAEA. doi:10.1594/PANGAEA.871017.

Maiersperger, T. K., P. L. Scaramuzza, L. Leigh, S. Shrestha, K. P. Gallo, C. B. Jenkerson, and J. L. Dwyer. 2013. "Characterizing LEDAPS Surface Reflectance

Products by Comparisons with AERONET, Field Spectrometer, and MODIS Data." *Remote Sensing of Environment* 136: 1–13. doi:10.1016/j.rse.2013.04.007.

Marfai, Muh Aris, Andung Bayu Sekaranom, and Philip Ward. 2014. "Community Responses and Adaptation Strategies toward Flood Hazard in Jakarta, Indonesia." *Natural Hazards* 75 (2): 1127–1144. doi:10.1007/s11069-014-1365-3.

Masek, J. G., F. E. Lindsay, and S. N. Goward. 2000. "Dynamics of Urban Growth in the Washington DC Metropolitan Area, 1973-1996, from Landsat Observations." *International Journal of Remote Sensing* 21 (18): 3473–3486. doi:10.1080/014311600750037507.

Masek, Jeffrey G, Eric F Vermote, Nazmi E Saleous, Robert Wolfe, Forrest G Hall, Karl F Huemmrich, Feng Gao, Jonathan Kutler, and Teng-kui Lim. 2006. "A Landsat Surface Reflectance Dataset." *IEEE Geoscience and Remote Sensing Letters* 3 (1): 68–72. doi:10.1109/LGRS.2005.857030.

Miller, Roberta Balstad, and Christopher Small. 2003. "Cities from Space: Potential Applications of Remote Sensing in Urban Environmental Research and Policy." *Environmental Science and Policy* 6 (2): 129–137. doi:10.1016/S1462-9011(03)00002-9.

Mountrakis, Giorgos, Jungho Im, and Caesar Ogole. 2011. "Support Vector Machines in Remote Sensing: A Review." *ISPRS Journal of Photogrammetry and Remote Sensing* 66 (3): 247–259. doi:10.1016/j.isprsjprs.2010.11.001.

Myint, Soe W., Patricia Gober, Anthony Brazel, Susanne Grossman-Clarke, and Qihao Weng. 2011. "Per-Pixel vs. Object-Based Classification of Urban Land Cover Extraction Using High Spatial Resolution Imagery." *Remote Sensing of*

Environment 115 (5): 1145–1161. doi:10.1016/j.rse.2010.12.017.

Pal, Mahesh, and Paul M. Mather. 2003. “An Assessment of the Effectiveness of Decision Tree Methods for Land Cover Classification.” *Remote Sensing of Environment* 86 (4): 554–565. doi:10.1016/S0034-4257(03)00132-9.

Pan, J, M Wang, D Li, and J Li. 2009. “Automatic Generation of Seamline Network Using Area Voronoi Diagrams With Overlap.” *IEEE Transactions on Geoscience and Remote Sensing* 47 (6): 1737–1744. doi:10.1109/TGRS.2008.2009880.

Powell, R, and D Roberts. 2008. “Characterizing Variability of the Urban Physical Environment for a Suite of Cities in Rondônia, Brazil.” *Earth Interactions* 12 (13): 1–32. doi:10.1175/2008EI246.1.

Powell, R, and D Roberts. 2010. “Characterizing Urban Land-Cover Change in Rondônia, Brazil: 1985 to 2000.” *Journal of Latin American Geography* 9 (3): 183–211. doi:10.1353/lag.2010.0028.

Powell, R, D Roberts, P Dennison, and L Hess. 2007. “Sub-Pixel Mapping of Urban Land Cover Using Multiple Endmember Spectral Mixture Analysis: Manaus, Brazil.” *Remote Sensing of Environment* 106 (2): 253–267. doi:10.1016/j.rse.2006.09.005.

Poznanska, Anna, Steven Bayer, and Tilman Bucher. 2013. “Derivation of Urban Objects and Their Attributes for Large-Scale Urban Areas Based on Very High Resolution UltraCam True Orthophotos and nDSM – a Case Study Berlin , Germany.” In *Proceedings of the SPIE*, 13. doi:10.1117/12.2030000.

Pravitasari, Andrea Emma, Izuru Saizen, Narumasa Tsutsumida, Ernan Rustiadi, and

Didit Okta Pribadi. 2015. “Local Spatially Dependent Driving Forces of Urban Expansion in an Emerging Asian Megacity: The Case of Greater Jakarta (Jabodetabek).” *Journal of Sustainable Development* 8 (1): 108–120. doi:10.5539/jsd.v8n1p108.

Ridd, M. K. 1995. “Exploring a V-I-S Model for Urban Ecosystem through Remote Sensing: A Comparative Ananomy for Cities.” *International Journal of Remote Sensing*.

Roscher, Ribana, Wolfgang Förstner, and Björn Waske. 2012. “I 2VM: Incremental Import Vector Machines.” *Image and Vision Computing* 30: 263–278. doi:10.1016/j.imavis.2012.04.004.

Roscher, Ribana, Björn Waske, and Wolfgang Forstner. 2010. “Kernel Discriminative Random Fields for Land Cover Classification.” *APR Workshop on Pattern Recognition in Remote Sensing*. doi:10.1109/PRRS.2010.5742801.

Schneider, A. 2012. “Monitoring Land Cover Change in Urban and Peri-Urban Areas Using Dense Time Stacks of Landsat Satellite Data and a Data Mining Approach.” *Remote Sensing of Environment* 124: 689–704. doi:10.1016/j.rse.2012.06.006.

Schneider, A, M A Friedl, and D Potere. 2009. “A New Map of Global Urban Extent from MODIS Satellite Data.” *Environmental Research Letters* 4 (4): 44003. doi:10.1088/1748-9326/4/4/044003.

Schneider, A, M Friedl, and D Potere. 2010. “Mapping Global Urban Areas Using MODIS 500-M Data: New Methods and Datasets Based on ‘Urban Ecoregions.’” *Remote Sensing of Environment* 114 (8): 1733–1746. doi:10.1016/j.rse.2010.03.003.

Schneider, A, and C M Mertes. 2014. “Expansion and Growth in Chinese Cities, 1978–2010.” *Environmental Research Letters* 9 (2): 24008. doi:10.1088/1748-9326/9/2/024008.

Schneider, A, K Seto, and D Webster. 2005. “Urban Growth in Chengdu, Western China: Application of Remote Sensing to Assess Planning and Policy Outcomes.” *Environment and Planning B: Planning and Design* 32 (3): 323–345. doi:10.1068/b31142.

Sexton, Joseph O., Xiao-Peng Song, Chengquan Huang, Saurabh Channan, Matthew E. Baker, and John R. Townshend. 2013. “Urban Growth of the Washington, D.C.–Baltimore, MD Metropolitan Region from 1984 to 2010 by Annual, Landsat-Based Estimates of Impervious Cover.” *Remote Sensing of Environment* 129: 42–53. doi:10.1016/j.rse.2012.10.025.

Sharifi, Ehsan, and Steffen Lehmann. 2014. “Comparative Analysis of Surface Urban Heat Island Effect in Central Sydney.” *Journal of Sustainable Development* 7 (3): 23–34. doi:10.5539/jsd.v7n3p23.

Song, Xiao-Peng, Joseph O. Sexton, Chengquan Huang, Saurabh Channan, and John R. Townshend. 2016. “Characterizing the Magnitude, Timing and Duration of Urban Growth from Time Series of Landsat-Based Estimates of Impervious Cover.” *Remote Sensing of Environment* 175: 1–13. doi:10.1016/j.rse.2015.12.027.

Sun, Genyun, Xiaolin Chen, Xiuping Jia, Yanjuan Yao, and Zhenjie Wang. 2015. “Combinational Build-Up Index (CBI) for Effective Impervious Surface Mapping in Urban Areas.” *IEEE Journal of Selected Topics in Applied Earth Observations and Remote Sensing*, 1–12. doi:10.1109/JSTARS.2015.2478914.

Sundarakumar, K, M Harika, S K Aspiya Begum, S Yamini, and K Balakrishna. 2012. "Land Use And Land Cover Change Detection And Urban Sprawl Analysis Of Vijayawada City Using Multitemporal Landsat." *International Journal of Engineering Science and Technology* 4 (1): 170–178.

Suryahadi, Asep, and Sudarno Sumarto. 2003. "Poverty and Vulnerability in Indonesia before and after the Economic Crisis." *Asian Economic Journal* 17 (1): 45–64. doi:10.1111/1351-3958.00161.

Turner, B, E Lambin, and A Reenberg. 2010. "The Emergence of Land Change Science for Global Environmental Change and Sustainability." *PNAS* 103 (128): 13070–13075. doi:10.1073/pnas.0704119104.

U.S. Department of Commerce. 2013. *2013 Housing Profile: United States*. *U.S. Department of Housing and Uban Development*. Washington, USA.

United Nations, Department of Economic and Social Affairs, Population Division. 2014. *World Urbanization Prospects: The 2014 Revision, Highlights (ST/ESA/SER.A/352)*. New York, NY, USA. doi:10.4054/DemRes.2005.12.9.

Varshney, Avnish, and Edida Rajesh. 2014. "A Comparative Study of Built-up Index Approaches for Automated Extraction of Built-up Regions From Remote Sensing Data." *Journal of the Indian Society of Remote Sensing* 42: 1–5. doi:10.1007/s12524-013-0333-9.

Vermote, E., D. Tanre, J.L. Deuze, M. Herman, and J.J. Morcrette. 1997. *Second Simulation of the Satellite Signal in the Solar Spectrum (6S). 6S User Guide Version 2. Appendix III: Description of the Subroutines*. Maryland, USA.

Wang, Liguo, Danfeng Liu, Qunming Wang, and Ying Wang. 2013. “Spectral Unmixing Model Based on Least Squares Support Vector Machine With Unmixing Residue Constraints” 10 (6): 1592–1596. doi:10.1109/LGRS.2013.2262371.

Wanner, W., X. Li, and a. H. Strahler. 1995. “On the Derivation of Kernels for Kernel-Driven Models of Bidirectional Reflectance.” *Journal of Geophysical Research* 100 (D10): 21077. doi:10.1029/95JD02371.

Watanachaturaporn, P, M K Arora, and P K Varshney. 2008. “Multisource Classification Using Support Vector Machines: An Empirical Comparison with Decision Tree and Neural Network Classifiers.” *Photogrammetric Engineering and Remote Sensing* 74 (2): 239–246. doi:10.14358/PERS.74.2.239.

Weng, Fenqing, and Ruiliang Pu. 2013. “Mapping and Assessing of Urban Impervious Areas Using Multiple Endmember Spectral Mixture Analysis: A Case Study in the City of Tampa, Florida.” *Geocarto International* 28 (7): 594–615. doi:10.1080/10106049.2013.764355.

Weng, Qihao. 2001. “Modeling Urban Growth Effects on Surface Runoff with the Integration of Remote Sensing and GIS.” *Environmental Management* 28 (6): 737–748. doi:10.1007/s002670010258.

Western Australian Planning Commission. 2013a. *The Housing We’d Choose: A Study for Perth and Peel*. *The Government of Western Australia Department of Housing and Department of Planning*. Perth,WA, Australia.

Western Australian Planning Commission. 2013b. *The Housing We’d Choose: A Study for Perth and Peel Summary Report*. Perth,WA, Australia.

Western Australian Planning Commission. 2015. *Perth and Peel @ 3.5 Million*. *The Government of Western Australia Department of Planning*. Perth,WA, Australia.

Wilson, Emily Hoffhine, James D. Hurd, Daniel L. Civco, Michael P. Prisloe, and Chester Arnold. 2003. "Development of a Geospatial Model to Quantify, Describe and Map Urban Growth." *Remote Sensing of Environment* 86 (3): 275–285. doi:10.1016/S0034-4257(03)00074-9.

Wu, C, and A T Murray. 2003. "Estimating Impervious Surface Distribution by Spectral Mixture Analysis." *Remote Sensing of Environment* 84: 493–505. doi:10.1016/S0034-4257(02)00136-0.

Xie, Qijiao, and Zhixiang Zhou. 2015. "Impact Of Urbanization On Urban Heat Island Effect Based On TM Imagery In Wuhan, China." *Environmental Engineering and Management Journal* 14 (3): 647–655.

Yuan, Fei, Kali E. Sawaya, Brian C. Loeffelholz, and Marvin E. Bauer. 2005. "Land Cover Classification and Change Analysis of the Twin Cities (Minnesota) Metropolitan Area by Multitemporal Landsat Remote Sensing." *Remote Sensing of Environment* 98 (2): 317–328. doi:10.1016/j.rse.2005.08.006.

Zhu, Ji, and Trevor Hastie. 2005. "Kernel Logistic Regression and the Import Vector Machine." *Journal of Computational and Graphical Statistics* 14 (2015): 185–205. doi:10.1198/106186005X25619.

Zhu, Zhe, and Curtis E. Woodcock. 2014. "Continuous Change Detection and Classification of Land Cover Using All Available Landsat Data." *Remote Sensing of Environment* 144: 152–171. doi:10.1016/j.rse.2014.01.011.

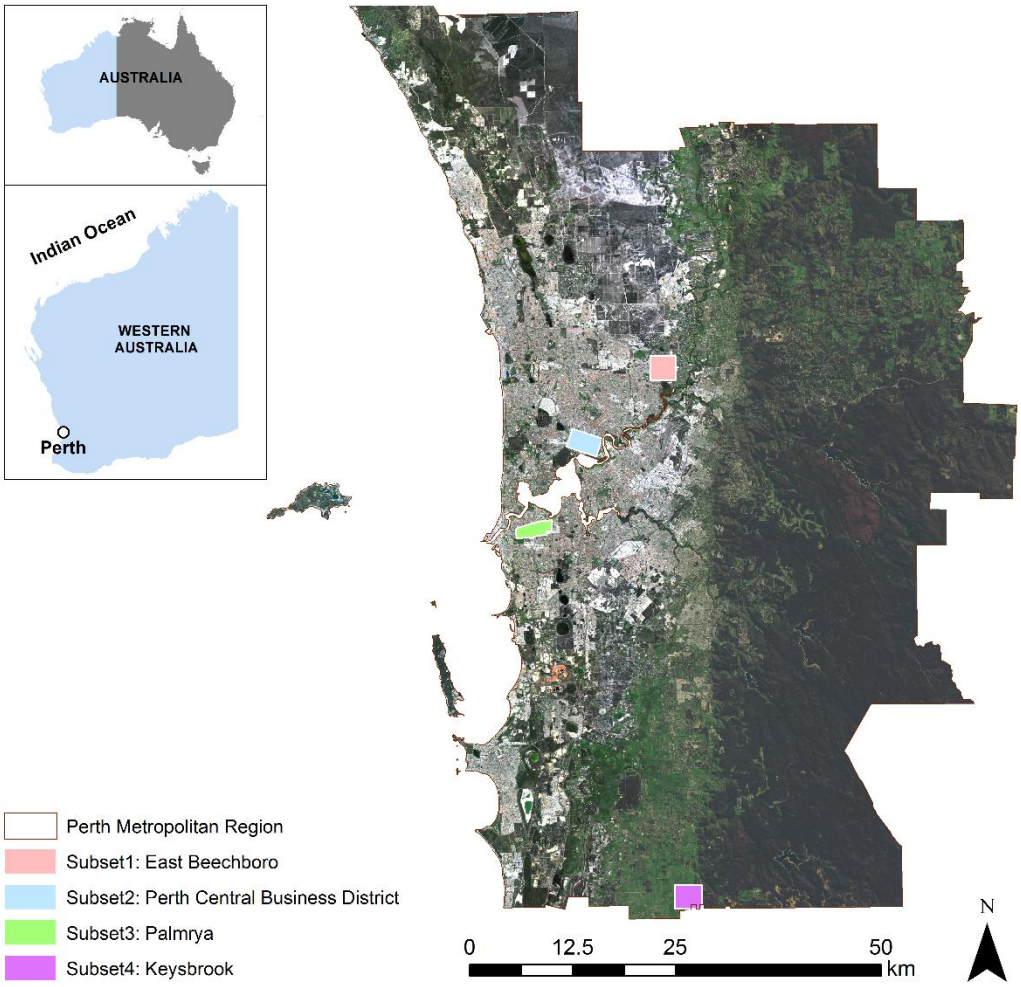

Figure 1. Landsat 8 Operational Land Imager (OLI) true colour image mosaic of the Perth Metropolitan Region (2015, August and September). The locations of the high spatial resolution aerial image subsets are indicated by coloured overlays.

Figure 2. Comparison of true colour high spatial resolution data (*a*, acquired in March 2007) and Landsat surface reflectance (*b*, acquaired in October 2007 (path 112), highlighting the spatial detail captured by high resolution imagery (*c*) and the same areas as observed by Landsat (*d*) for the subset East Beechboro used within this study.

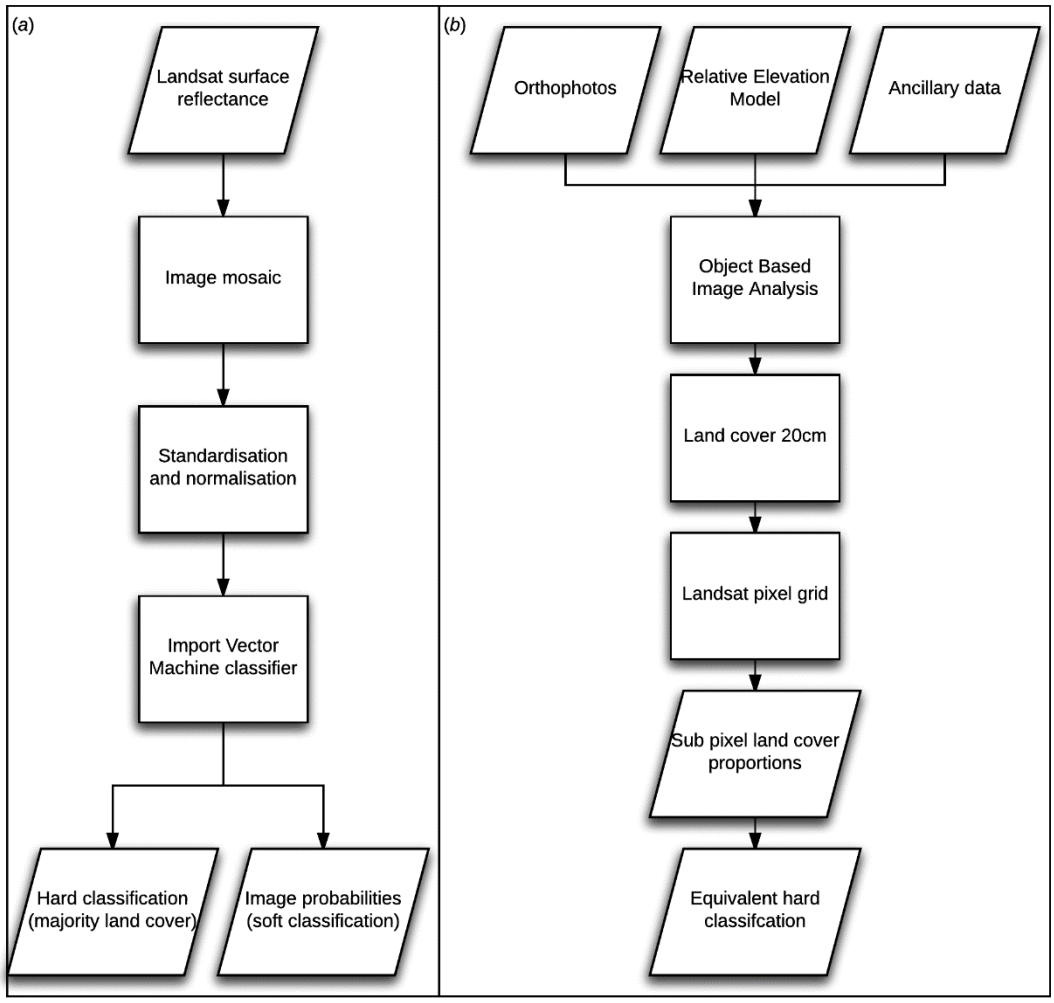

Figure 3. Summary of classification procedures for (*a*) Landsat and (*b*) high resolution orthophoto data.

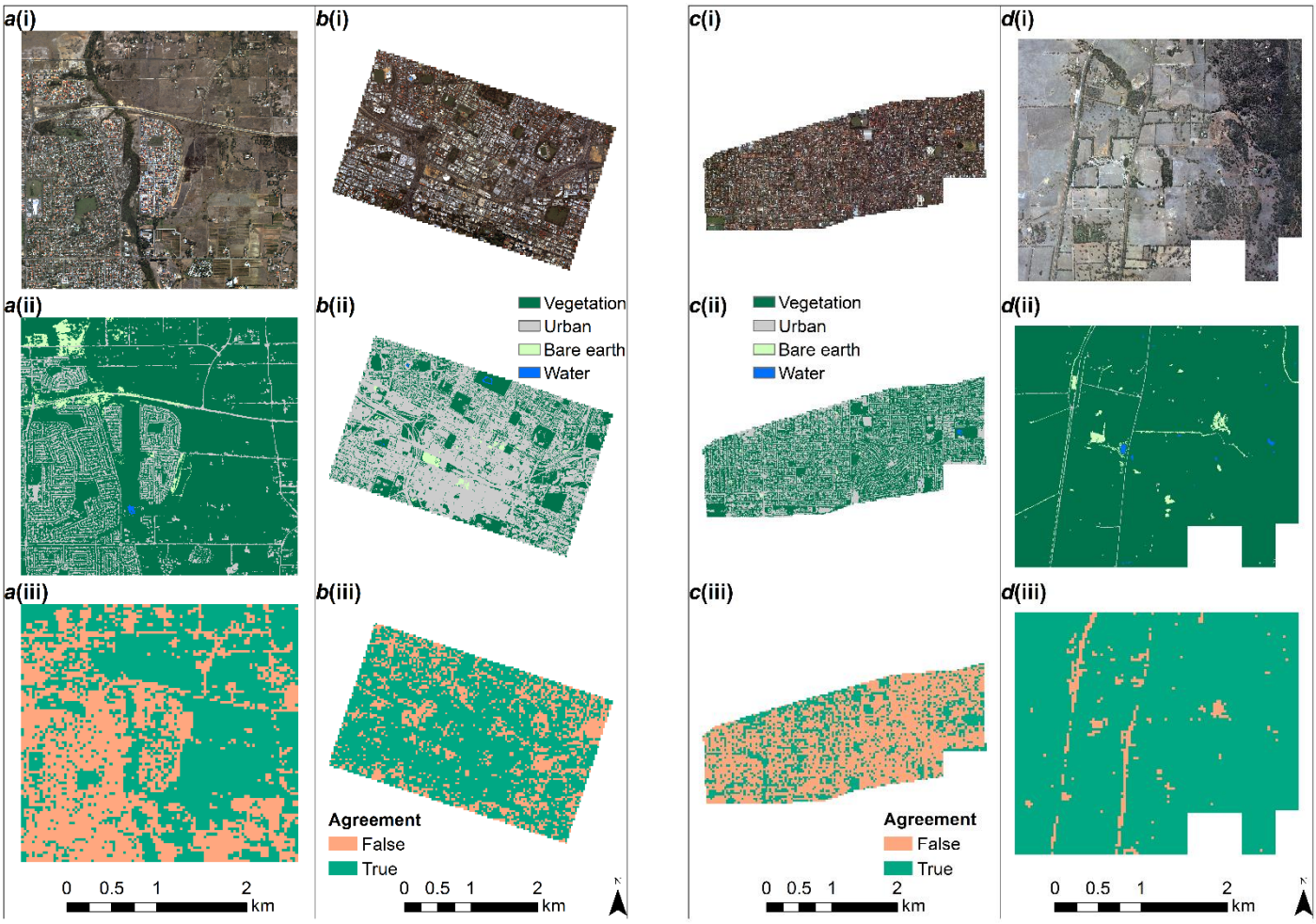

Figure 4. (i) High spatial resolution true colour orthophotos, (ii) land cover maps and (iii) the agreement between the orthophoto classification resampled to 30 m^2 and the Landsat classification for: (*a*) an out of town development area (East Beechboro), (*b*) old inner city urban area (Central Business District), (*c*) older suburban area (Palmrya, Melville) and (*d*) predominantly vegetated site (Keysbrook). In (iii), areas depicted as '*true'* indicate those 30 m^2 pixels where the orthophoto land cover type, based on the dominant land cover in the 30 m^2 area, and Landsat land cover type are in agreement.

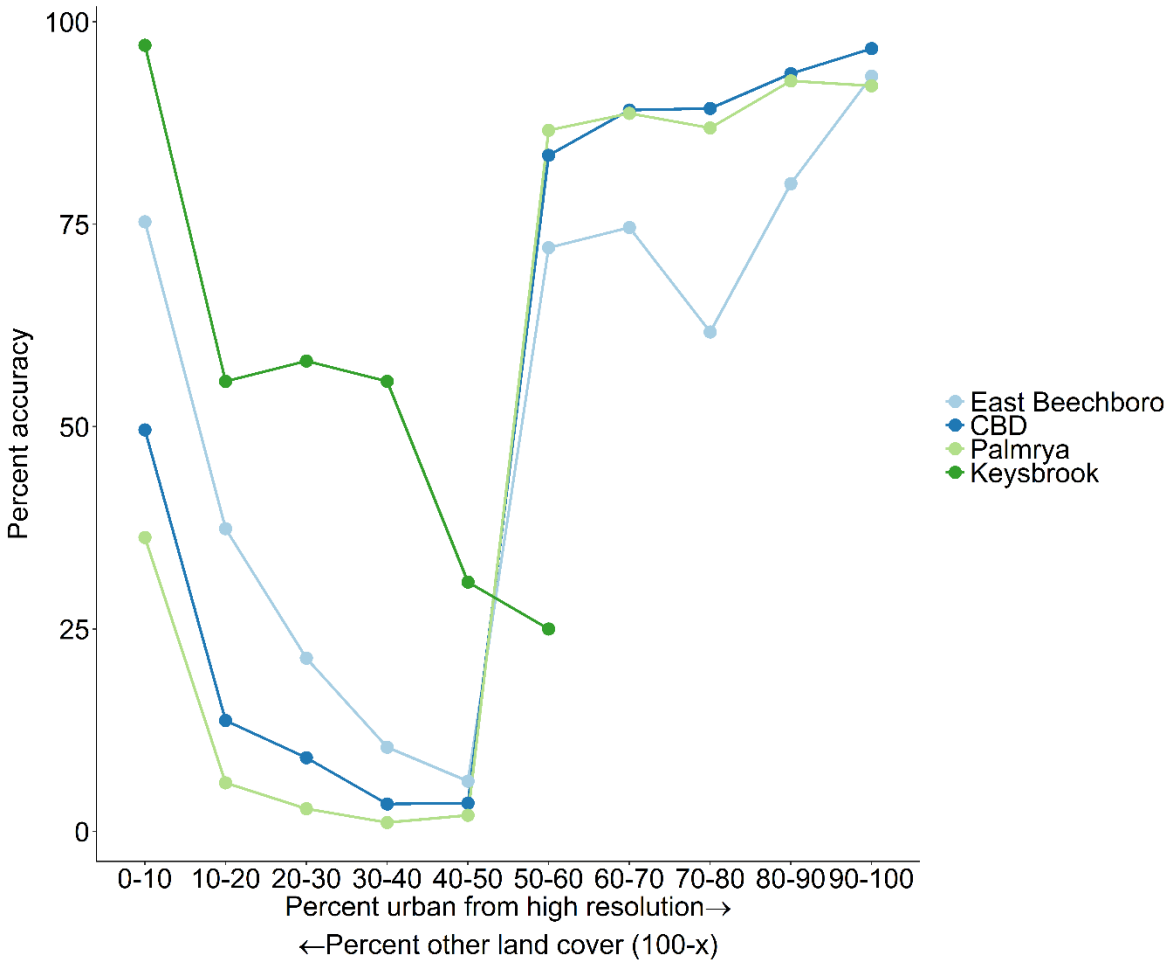

Figure 5: Landsat classification accuracy as a function of the percentage urban cover within Landsat image pixels (as derived from the high spatial resolution land cover dataset) for each of the four subsets. In the Keysbrook subset no Landsat pixels contained >60% urban land cover.

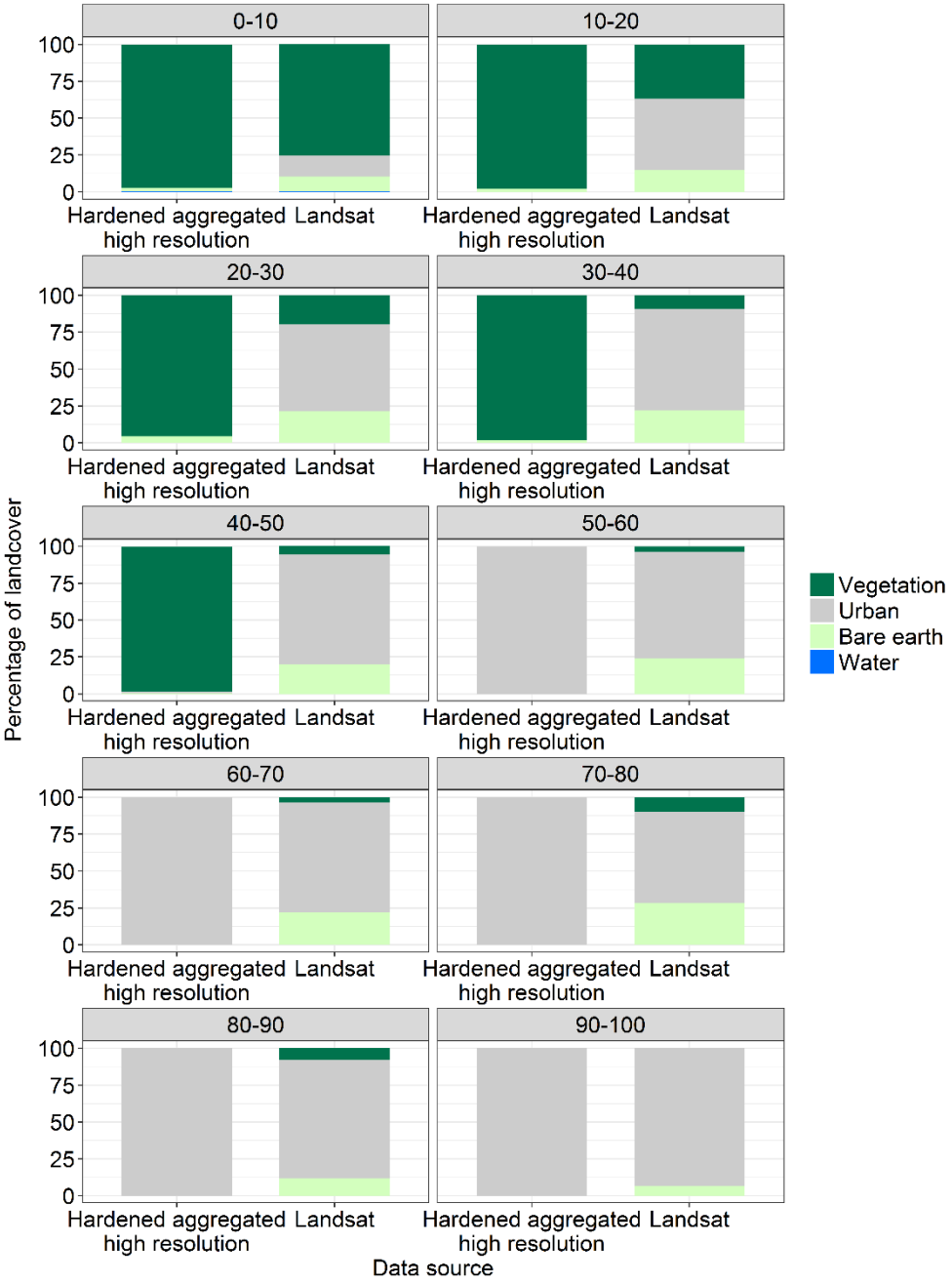

Figure 6. Land cover type disaggregation for urban land cover (according to the orthophoto imagery) Landsat pixels in East Beechboro. The left axis indicates the total percentage cover of a given land cover type using all of the pixels within a given range of urban percentage cover range (e.g. 0-10%, 10-20%). For each percentage urban land cover graph, the left bar illustrates the overall percentage of pixels from the hardened high spatial resolution classification identified as a given land types whilst the right bar indicates the percentage of hardened Landsat pixels mapped as a given land cover type.

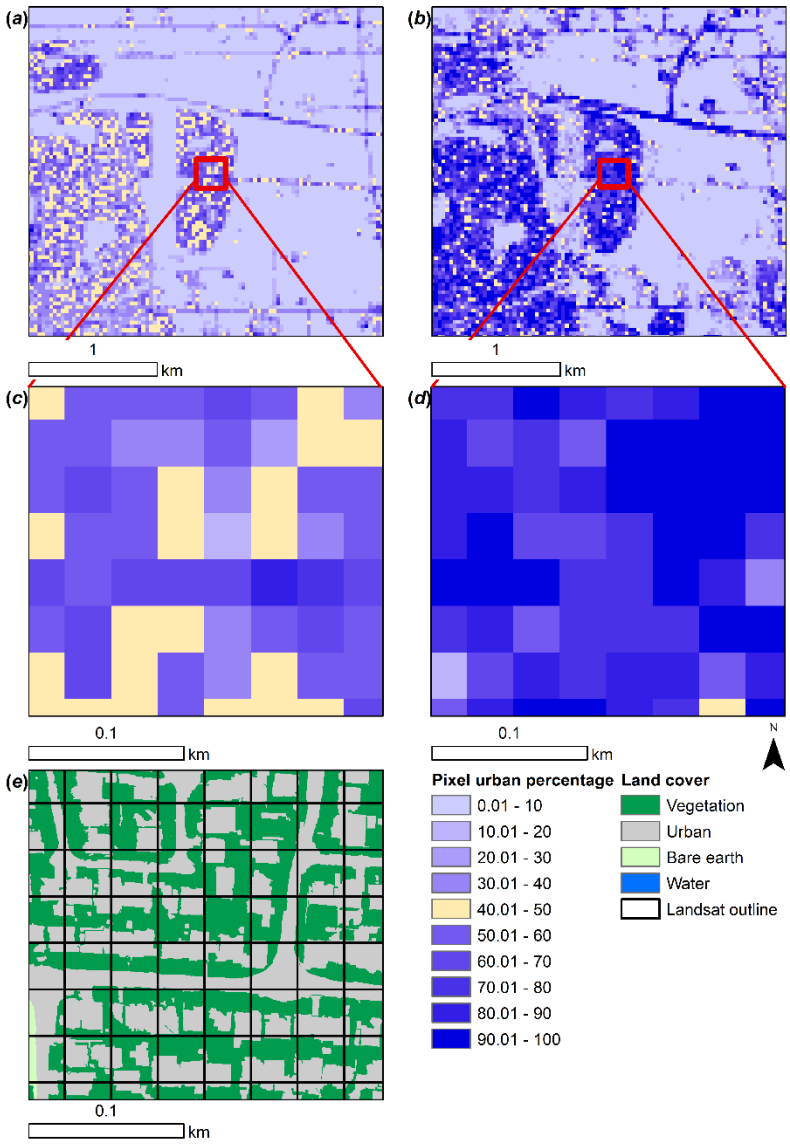

Figure 7. Comparison of percentage urban area aggregated to 30 m^2 from high resolution data (a) and IVM 'soft' Landsat classification (b) highlighting the (overestimation) between the high (c) and moderate (d) spatial resolution estimates for the East Beechboro subset. The classified high spatial resolution data is shown in (e) with the moderate spatial resolution grid (30 m^2) overlaid for context (e).

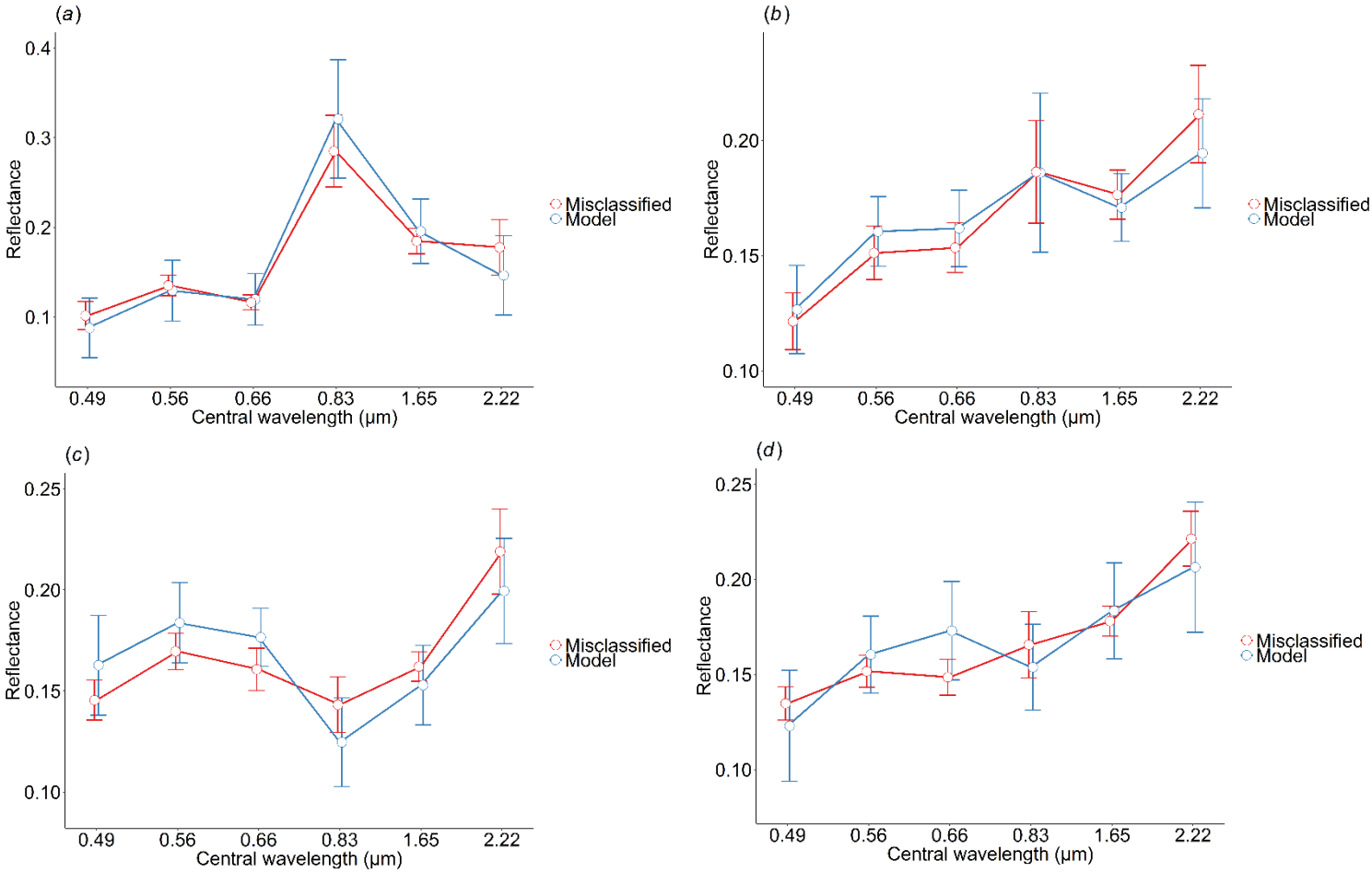

Figure 8. Average spectral reflectance profile for misclassified pixels (red) from the Palmrya subset for pixels containing 20-30% urban cover compared to the average spectral reflectance profile of pixels used to train the IVM classification algorithm (blue). For (*a*) forest (*b*) low urban reflectance (*c*) high urban reflectance and (*d*) bare earth. The error bars show the standard deviation.

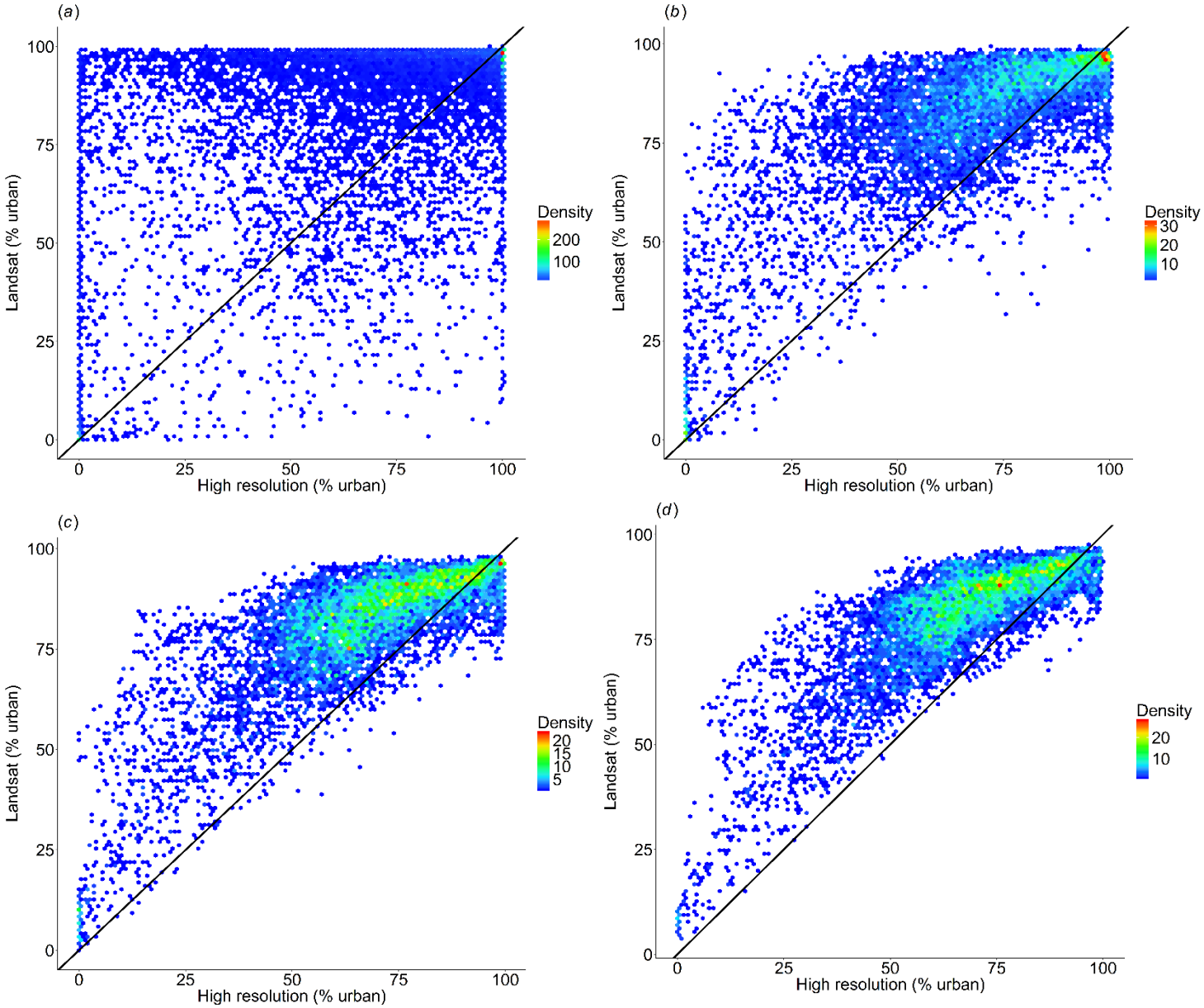

Figure 9. Relationship between the sub-pixel urban area percentage cover estimated from the IVM sub-pixel Landsat classification and the high spatial resolution orthophoto classification in the Central Business District (CBD) subset for (*a*) 30×30 m window, (*b*) 90×90 m window, (*c*) 150×150 m window and (*d*) 210×210 m window.

Subset	Vegetation	Urban	Bare earth	Water
East Beechboro	16.56	81.0	2.37	0.07
CBD	33.33	65.66	0.91	0.1
Palmrya	42.21	57.29	0.42	0.08
Keysbrook	97.36	0.90	1.56	0.18

Table 1. The percentage of different land cover types within the classified high spatial resolution subsets (Figure 1).

Subset	Vegetation	Urban	Bare earth	Water
East Beechboro	87.57	9.84	1.89	0.06
CBD	26.14	72.81	0.74	0.05
Palmrya	66.71	32.33	0.21	0.07
Keysbrook	98.90	0.05	0.88	0.11

Table 2. The percentage of pixels which contain >50% of a given land cover type in each region.

Subset	High resolution urban area (km^2)	Percentage cover of subset area	Landsat urban area (km^2)	Percentage cover of subset area	Percent difference to high resolution	Landsat urban area sub-pixel (km^2)	Percentage cover of subset area	Percent difference to high resolution
East Beechboro	1.47	16.56	3.22	36.21	118.66	3.12	35.06	111.69
CBD	5.58	65.66	7.28	85.71	30.55	6.78	79.85	21.62
Palmrya	2.70	42.21	5.50	85.94	103.65	4.90	76.55	81.42
Keysbrook	0.08	0.9	0.28	3.17	251.74	0.29	3.30	266.26

Table 3. Urban area estimates (km^2) from high spatial resolution orthophoto land cover data for each subset and those from the corresponding hard and soft IVM Landsat classification. The overestimation of urban area by the hardened Landsat land cover classification is evident.

Subset	Vegetation (%)	Urban (%)	Bare earth (%)	Water (%)
East Beechboro	53.93	0.15	0.34	0.03
CBD	8.98	28.77	0.35	0.00
Palmrya	5.80	2.13	0.00	0.01
Keysbrook	92.05	0.00	0.00	0.00

Table 4. Percentage of 'pure' pixels (defined here as comprising 90-100% of given landcover within a Landsat pixel area) from the high spatial resolution imagery.

Subset	Kernel size (m)	Coefficient of determination (R^2)	Scatter	Bias	Root Mean Square Error (RMSE)
East Beechboro	30×30	0.41*	26.65	18.68	32.54
	90×90	0.68*	16.95	18.66	25.21
	150×150	0.75*	14.11	18.71	23.44
	210×210	0.80*	12.52	18.74	22.54
CBD	30×30	0.26*	28.41	14.38	31.84
	90×90	0.53*	16.65	14.37	22.00
	150×150	0.61*	13.18	14.38	19.51
	210×210	0.66*	11.30	14.36	18.28
Palmrya	30×30	0.04*	26.65	34.54	43.62
	90×90	0.16*	13.56	34.61	37.17
	150×150	0.19*	10.15	34.64	36.10
	210×210	0.17*	8.45	34.67	35.69
Keysbrook	30×30	0.24*	11.85	2.51	12.11
	90×90	0.52*	7.47	2.51	7.88
	150×150	0.60*	5.89	2.50	6.40
	210×210	0.63*	4.98	2.50	5.57

Table 5. Comparison between high (20 cm^2) and moderate (30 m^2) spatial resolution sub-pixel impervious surface estimates considering differing kernel sizes over four subsets (Figure 1) within the PMR. * = statistically significant relationship ($p<0.05$).

Subset	Coefficient of determination (R^2)	Bias	Root Mean Square Error (RMSE)	High resolution urban (km^2)	Uncorrected Landsat urban (km^2) and percent difference to high resolution	Corrected Landsat urban (km^2) and percent difference to high resolution
East Beechboro	0.84*	1.54	6.76	2.49	5.32 (72.47%)	2.72 (8.83%)
CBD	0.52*	-7.12	14.61	12.26	15.36 (22.45%)	10.88 (-11.93)
Palmrya	0.12*	7.43	12.53	6.92	12.48 (57.32)	8.10 (15.71)
Keysbrook	0.62*	0.37	1.38	0.133	0.50 (115.96)	0.19 (35.29)

Table 6. Comparison between calibrated moderate (30 m^2) and high (20 cm^2) resolution sub-pixel impervious surface estimates with a kernel size of 210m. * = statistically significant relationship ($p<0.05$).